Welding in the World
https://doi.org/10.1007/s40194-025-02030-5

RESEARCH PAPER

Delta ferrite in modified 9Cr–1Mo steel weld metal

Sibusiso Mahlalela[1] · **Pieter Pistorius**[1]

Received: 25 October 2024 / Accepted: 24 March 2025

Abstract
The role of chemical composition on the presence of δ-ferrite in P91 weld metal in the as-welded condition was studied by systematically varying five alloying elements (Cr, Ni, Mn, Si, and Mo) in 28 gas–metal arc welds. The effect of thermal treatment on the δ-ferrite content was also investigated. Metallography analysis of the as-welded beads showed that 18 of the 28 welds contained 0.3 to 6.2% δ-ferrite in martensite. Sixteen of the 28 welds fully complied with chemical composition specifications, including the limit of the sum of (Mn + Ni). Of the sixteen welds that complied with the AWS A5.28/A5.28 M:2022 (ER90S-B91) chemical composition specification, thirteen contained δ-ferrite. Based on these results, lower specification limits for Mo and Si are proposed to ensure a fully martensitic microstructure. Empirical formulae were applied to evaluate their accuracy in predicting the P91 as-welded microstructure: ten of the 28 welds (36%) were incorrectly predicted. Based on these results, the recommended Schaeffler Cr_{eq} and Kaltenhauser ferrite factor maximum limits should be lowered to 11.5 and 6, respectively, to limit the presence of δ-ferrite in the P91 as-welded microstructure. Phase-transformation temperatures were evaluated against the amount of δ-ferrite in beads in the as-welded condition. It was observed that a wider $(Ae_4 - Ae_3)$ temperature range was beneficial in suppressing δ-ferrite in the final as-welded microstructure. Higher peak temperatures and slower cooling rates during welding also reduced the amount of δ-ferrite in P91 weld metal.

Keywords 9Cr–1Mo (P91) steel · Delta ferrite · Gas–metal arc welding · Direct laser deposition · Thermo-Calc simulation

1 Introduction

Modified 9Cr–1Mo steel, also known as P91 steel, finds broad application in services that require good creep properties [1]. Thermomechanical processes during fabrication of P91 steel should be such that a fully martensitic microstructure is achieved, free of delta (δ) ferrite. The presence of δ-ferrite is generally viewed as detrimental to mechanical properties. Anderko et al. [2] and Abe et al. [3] reported impact toughness results, showing that an increase in δ-ferrite amount led to a lower upper-shelf energy and higher ductile–brittle transition temperature (DBTT). Amounts less than 2% of δ-ferrite were shown to have no significant effect on the room-temperature tensile strength but slightly improved elongation [4]. Laha et al. [5] investigated hot tensile properties in P91 weldments and observed that the presence of δ-ferrite restricted grain growth, increased strength, and decreased ductility. The presence of δ-ferrite was reported to be detrimental to long-term creep-rupture properties of P91 steel, even with a volume fraction as low as 2%, but not to short-term creep-rupture strength [4, 6, 7].

Delta ferrite is the primary phase that forms from liquid at the start of solidification. With further cooling below the Ae_5 temperature, the austenite phase will transform from δ-ferrite. Austenite in P91 steel transforms to a fully martensitic structure at cooling rates > 0.2 °C/s, which are well below typical cooling rates experienced during welding [8]. The equilibrium transformation temperatures are defined as follows (on heating) [9]: Ae_1: onset of austenite formation; Ae_3: fully austenitic phase is achieved; Ae_4: onset of δ-ferrite formation from austenite; and Ae_5: completion of austenite-to-delta ferrite transformation. The $(Ae_4 - Ae_3)$ temperature range is the region where only the austenite phase is

Recommended for publication by Commission IX - Behaviour of Metals Subjected to Welding

✉ Sibusiso Mahlalela
sibusiso.mahlalela@up.ac.za

Pieter Pistorius
pieter.pistorius@up.ac.za

[1] Department of Materials Science and Metallurgical Engineering, Southern African Institute for Welding Centre for Welding Engineering, University of Pretoria, Gauteng, Pretoria, South Africa

Published online: 03 April 2025

Table 1 Chemical composition (%) of P91 base material steel pipe and filler wire, as provided by the supplier

Element	*P91 steel (%)*		*P91 weld metal (%)*		
	ASTM A335/ A335M-21	*Base material*	*AWS A5.28/* A5.28 M:*2022 (E90S-B91)*	*ISO 21952:2012 (CrMo91)*	*Filler wire*
	Min – max		*Min – max*	*Min – max*	
C	0.08 – 0.12	0.11	0.07 – 0.13	0.07 – 0.15	0.10
Mn	0.30 – 0.60	0.53	– 1.20	0.40 – 1.50	0.60
Cr	8.00 – 9.50	8.21	8.00 –10.50	8.00 – 10.50	8.80
Si	0.20 – 0.50	0.33	0.15 – 0.50	– 0.60	0.24
Mo	0.85 – 1.05	0.93	0.85 – 1.20	0.80 – 1.20	0.94
V	0.18 – 0.25	0.24	0.15 – 0.30	0.15 – 0.30	0.20
Nb	0.06 – 0.10	0.10	0.02 – 0.10	0.03 – 0.10	0.06
N	0.03 – 0.07	0.06	0.03 – 0.07	0.02 – 0.07	0.04
Ni	– 0.40	0.25	– 0.80	0.40 – 1.00	0.50
Al	– 0.02	0.005	– 0.04	–	–

stable under equilibrium conditions. Arivazhagan et al. [10] stated that the probability of δ-ferrite retention in the weld increases with a lower ($Ae_4 - Ae_3$) temperature range value.

The generally observed influence of cooling rate on the volume fraction of δ-ferrite in as-welded final microstructures is that slower cooling rates reduce the amount of residual δ-ferrite [11], but there are instances where this rule does not apply [12]. The duration within the (δ + γ) and γ-only phase regions determines the completion of the transformation from δ-ferrite to austenite. Increased time spent in these phase fields reduces the amount of δ-ferrite retained in the final weld microstructure. On the contrary, Arivazhagan et al. [13] stated that a very high cooling rate associated with low heat input may result in a complete absence of δ-ferrite in the final microstructure.

The retention of δ-ferrite in the weld metal is often predicted from the chemical composition using modifications of the Schaeffler, Schneider, Kaltenhauser, and Newhouse empirical formulas [14], with certain recommended maximum values. Delta ferrite in P91 as-welded microstructures is often observed in alloys with chromium equivalent (Cr_{eq}) and ferrite factor (FF) values well below the recommended values [15]. This investigation focused on examining the role of chemical composition on the presence of δ-ferrite, with the objective of making recommendations on avoiding δ-ferrite in P91 weld metal in the as-welded condition. Empirical values from the weld compositions of this study were analysed to evaluate the recommended empirical limits. An important objective was also to determine if δ-ferrite can be observed in as-welded microstructures of P91 weld metal that fully complied with the chemical composition requirements of weld metal AWS A5.28/A5.28 M:2022 (ER90S-B91) and *ISO 21952:2012 (CrMo91)* specifications [16, 17]. The AWS A5.28/A5.28 M:2022 (ER90S-B91) standard was extracted from the ASME PBVC.II.C-2023 specification. The use of preheating during welding and experimental techniques like Gleeble simulation was applied in this research to examine the effect of the weld thermal cycles on the presence of δ-ferrite in the weld structure.

2 Experimental procedures

2.1 Thermo-Calc simulation

A series of 130 variations of weld metal compositions within the AWS A5.28/A5.28 M:2022 (ER90S-B91) chemical specification were evaluated by Thermo-Calc simulations using the TCFE7 database [18]. The objective was to utilise the information to select the alloying elements that have the most effect on (a) observed δ-ferrite, (b) empirical values (Cr_{eq}, Ni_{eq}, FF, chromium-nickel balance (CNB)), and (c) transformation temperature.

2.2 Welding

The study was done by altering the weld metal composition and cooling rate during welding. A seamless pipe of X10CrMoVNb9 – 1(P91) steel grade with heat number 223399 was used as the base material. Table 1 shows the chemical compositions of the base material and the Böhler C 9 MV-UP filler wire used as the gas–metal arc welding (GMAW) filler material. The supplier provided the chemical composition of the filler wire, which was 1.2 mm in diameter.

To meet the objectives of the study, 28 GMA welds of varying compositions were deposited on a P91 steel pipe. The Thermo-Calc results were utilised to select five alloying elements (Cr, Ni, Mn, Si, and Mo), which were varied in the 28 GMA weld alloy compositions. Systematic variations in the chemical composition of the GMAW beads

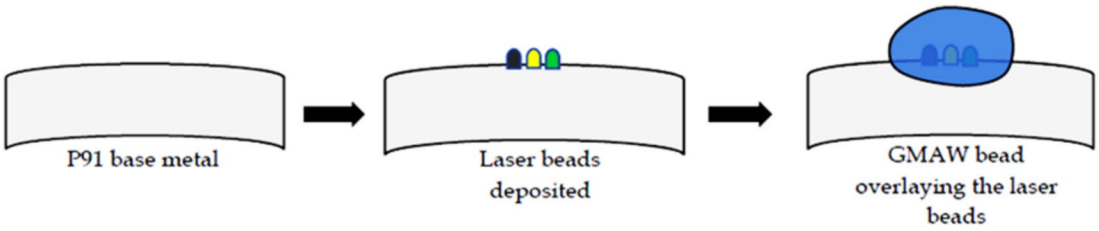

Fig. 1 Schematic illustration of alloying technique to systematically vary the chemical composition of the gas–metal arc weld beads

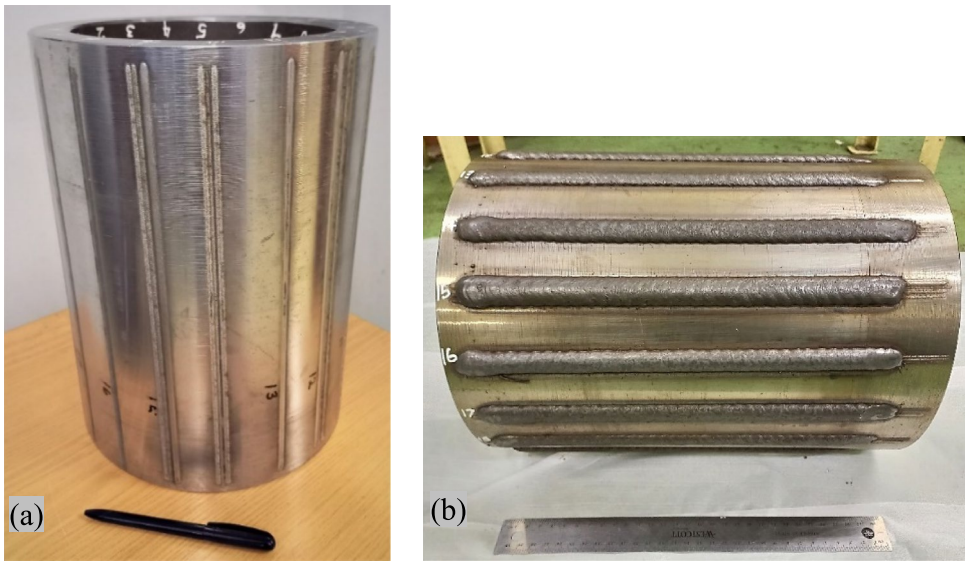

Fig. 2 **a** Preliminary laser beads of different elements deposited on the seamless P91 steel pipe. **b** P91 pipe with gas–metal arc welded beads. The 30 cm ruler in image **b** is for scale reference

were achieved by first depositing laser beads of the different alloying metal powders prior to overlaying these with a single-pass GMAW bead, as illustrated in Fig. 1. All welds were bead-on-plate welds. Each laser bead was deposited according to a specific target composition, with the aim of achieving a GMAW bead that met the requirements of the AWS A5.28/A5.28 M:2022 (ER90S-B91) specification.

All welds were performed with the same parameters to ensure consistency in heat input during GMAW. The welding process was semi-automated, with the torch fixed to an arm controlled by the rail-runner welding carriage. The welding parameters were as follows: welding speed was 20 cm/min, wire feed speed was 13.2 m/min, welding current was 218A, and the welding voltage was 28.5 V. A weaving welding path was applied to ensure wider GMAW beads sufficiently covered the laser alloying beads. The shielding gas was Ar with 2% O_2 at a flow rate of 15 L/min. Six welds, designated PH 1 to PH 6, were performed at a preheat temperature of 250 °C. Twenty-two welds, designated AW 1 to AW 22, received no preheating. Heat input (HI) was calculated from the total energy (from the power supply) and the bead length, applying a 0.85 arc efficiency (η) [19]:

$$HI\ (kJ/mm) = \eta \times total\ energy\ (kJ) \ /\ bead\ length\ (mm) \quad (1)$$

The heat input ranged from 1.4 to 1.7 kJ/mm.

Figure 2a shows multiple laser beam welds of different alloys deposited along the length of the P91 steel pipe; Fig. 2b shows the laser beads overlaid with a single-pass GMA weld. The estimated cooling rates calculated from the Rosenthal cooling time ($\Delta t8\text{-}5$) of the preheated welds and the non-preheated welds were 60 and 95 °C/s, respectively.

2.3 Characterisation

For consistency of the reported chemical compositions and microstructures of all 28 welds, the analysed specimens were removed at the same position along the length of all weld beads. Chemical compositions of the GMAW beads were analysed by an external accredited laboratory using optical emission spectroscopy (OES). In addition, four of the 28 GMA welds were selected and their compositions analysed (OES) in five positions about 40 mm apart along the weld bead length to determine the uniformity of chemical composition along the bead length.

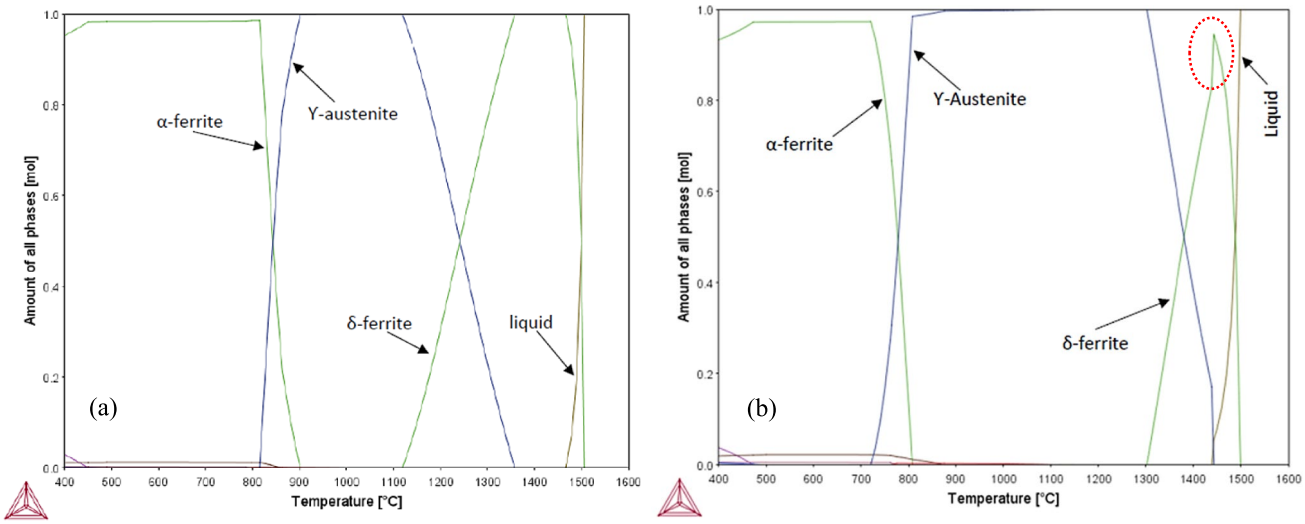

Fig. 3 P91 property diagrams constructed using Thermo-Calc software, showing the mole fractions of phases as a function of temperature. **a** Transformation sequence where the liquid transforms to 100% δ-ferrite phase during cooling and **b** P91 alloy with high austenite-formers. Austenite begins forming before solidification is completed and is referred to as a peritectic transition, highlighted by the red circle [9]

To reveal the microstructural constituents after specimen preparation, etching was performed using Villella's reagent (100 mL ethanol, 1 g picric acid, 5 mL HCl). Delta ferrite phase fraction was quantified by the point-counting method. Over 20 micrograph images per weld were analysed (100× magnification), covering the transverse cross-section of the GMAW bead.

Gleeble thermal treatment was performed to simulate the thermal cycle experienced by a weld bead when a subsequent bead is deposited in a multiple-pass weld. Five welds that contained significant amounts of δ-ferrite in the as-welded condition were selected. Specimens were machined from the weld metal to a rectangular prism (15 mm × 7 mm × 10 mm (L × H × W)) with rounded edges. The thermal cycle experienced by the reheated weld metal was physically simulated to peak temperatures of 1350, 1100, and 900 °C using a Gleeble 1500 thermo-mechanical simulator. Heating and cooling rates of 300 °C/s and 25 °C/s, respectively, were applied, with no holding time at peak temperature.

3 Results and discussion

3.1 Thermo-Calc estimate of phase equilibria

3.1.1 Transformation between liquidus and solidus temperatures

The phase-transformation sequence can take two slightly different routes during cooling, depending on the balance between austenite- and ferrite-forming elements in the composition of the P91 weld metal based on Thermo-Calc results analysis, as shown by the property diagrams in Fig. 3 [9].

In the first transformation sequence (Fig. 3a), with higher amounts of ferrite-forming elements in P91 alloy, the liquid transforms to 100% δ-ferrite during cooling:

$$Liquid \rightarrow liquid + \delta \rightarrow \delta \quad (2)$$

In the second transformation sequence (Fig. 3b), austenite begins forming before solidification is complete; this phase evolution is referred to as a peritectic transition [15]. A peritectic reaction occurs when the liquid and δ-ferrite phases transform to austenite and δ-ferrite at the Ae_5 temperature:

$$Liquid \rightarrow liquid + \delta \rightarrow \delta + \gamma \quad (3)$$

3.1.2 Transformation below solidus temperature

With further cooling below the Ae_5 temperature, austenite nucleates and grows from the δ-ferrite ($\delta \rightarrow \delta + \gamma$) or the peritectic reaction occurs in which the liquid and δ-ferrite phases transform to austenite and δ-ferrite ($liquid + \delta \rightarrow \delta + \gamma$). The growth of austenite during cooling is mainly controlled by diffusion. Villaret et al. [20] demonstrated that the nucleation of austenite is delayed to lower temperatures at fast cooling rates, and the grain growth rate is reduced because of the slow diffusion of interstitial elements like C.

3.1.3 Transformation below Ae_4 temperature

The completion of austenite formation is expected to be achieved under equilibrium conditions, but a higher cooling rate and delayed nucleation of austenite to lower temperatures could mean that the presence of δ-ferrite persists below the Ae_4 temperature and, as observed in this study, δ-ferrite may persist to ambient temperature. A large ($Ae_4 - Ae_3$) value, which is dependent on the P91 composition, is beneficial in allowing more time for completion of the δ-ferrite → austenite transformation above the Ae_3temperature.

3.1.4 Transformation between Ae_3 and ambient temperature

Under equilibrium conditions, α-ferrite nucleates and grows from austenite. The austenite → α-ferrite transformation is completed at the Ae_1 temperature. Under non-equilibrium conditions, δ-ferrite present below Ae_3 becomes stable and will be retained during cooling to ambient temperatures. Any retained austenite transforms to martensite (α') below the M_s temperature. The two possible transformation sequences under non-equilibrium cooling, where δ-ferrite is retained at room temperature, are as follows:

$$Liquid \rightarrow liquid + \delta \rightarrow \delta \rightarrow \delta + \gamma \rightarrow \gamma + \delta \rightarrow \alpha' + \delta \quad (4)$$

or.

$$Liquid \rightarrow liquid + \delta \rightarrow \delta + \gamma \rightarrow \gamma + \delta \rightarrow \alpha' + \delta \quad (5)$$

3.2 Chemical composition of welds

Table 2 presents the alloying elements added to each GMAW bead and the resultant chemical compositions of the welds. Welds PH 1 and AW 1 comprised only the GMAW filler wire deposit (i.e., without additional laser beads). Seven welds, highlighted in Table 2, exceeded the upper limit of the elemental specification range and thus did not fully comply with the AWS A5.28/A5.28 M:2022 (ER90S-B91) specification. This standard does not specify minimum requirements for Mn and Ni but does specify that their sum (Mn + Ni) shall be 1.4% maximum. The AWS A5.28/A5.28 M:2022 (ER90S-B91) specification further restricts the (Mn + Ni) content to 1.2%, for B91(1.2) and to 1.0 for the B91 (1.0%). Seven additional welds had a content above the 1.4% (Mn + Ni) limit.

3.3 Metallography of weld beads in as-welded condition

The volume fractions of δ-ferrite in the weld microstructures are presented in Table 3. Four of the six welds that received preheat treatment were fully martensitic. Welds PH 4 and PH 5 consisted of a martensitic matrix with 0.3% and 3.5% δ-ferrite, respectively. Weld PH 4 contained two additional laser beads of Cr, which is a strong ferrite former, and two laser beads of Mn, which is an austenite stabiliser. The opposing effects of Cr and Mn limited the observed δ-ferrite in PH 4. Weld PH 5 contained additional Mo and Cr, both strong ferrite-formers, and a single laser bead of Mn.

Only six of the 22 welds (AW 1, 7, 8, 12, 13, and 22) that received no preheat treatment were fully martensitic. AW 1 was deposited without any laser bead alloying. Ni contents in welds AW 7 and AW 8 were above the AWS specification limit because of the added Ni (strong austenite-former) laser beads. Welds AW 12, AW 13, and AW 22 contained additional Mn and had no additional Cr laser beads.

Welds AW 2, AW 11, AW 14, and AW 20 contained less than 0.5% volume fraction of small polygonal δ-ferrite grains. The chemical compositions of these four welds complied with the AWS A5.28/A5.28 M specification, yet their microstructures contained δ-ferrite. Eight welds, namely, AW 3, AW 4, AW 6, AW 10, AW 15, AW 18, AW 19, and AW 21, contained δ-ferrite volume fractions between 1 and 2.6%. Figure 4a shows a microstructure image of AW 19, which contained 2.4% δ-ferrite in a martensitic matrix. All eight welds contained laser beads of both ferrite- and austenite-forming elements. Six of the eight welds complied with the AWS A5.28/A5.28 M:2022 composition specification. The remaining four welds (AW 5, AW 9, AW 16, and AW 17) contained between 3.8 and 6.2% δ-ferrite. Figure 4 shows a microstructure image of AW 17, which contained 6.2% δ-ferrite. The δ-ferrite morphology was a mixture of small to large polygonal grains and fine elongated grains. Welds AW 9 and AW 16 complied with the composition specification yet contained significant amounts of δ-ferrite.

Sixteen of the 28 GMA welds complied with AWS A5.2/A5.28 M:2022 composition elemental range limits. Thirteen of these 16 welds contained δ-ferrite in their microstructures. Eight of these thirteen welds contained more than 1% δ-ferrite.

3.4 Delta ferrite content as a function of transformation temperature

The relationship between the Ae_1, Ae_3, Ae_4, and Ae_5 transformation temperatures (as determined by Thermo-Calc) and the amount of δ-ferrite in the final microstructure of the welds was examined. The transformation temperatures (Ae_1, Ae_3, Ae_4, and Ae_5), when considered as single parameters, did not have a significant predictive capability, but welds with $Ae_1 < 780$ °C, $Ae_3 < 840$ °C, and $Ae_4 \geq 1260$ °C were observed to contain no δ-ferrite. A low Ae_1 temperature that is close to the recommended PWHT (760 °C) temperature is not desirable because it increases the risk

Table 2 Metal alloys deposited and compositions (mass%) of GMAW beads (AWS A5.28/A5.28 M:2022 (ER90S-B91) specification). Elements above the specified limits are highlighted

GMAW beads	*Alloying added (number of laser beads deposited)*	*C*	*Mn*	*Cr*	*Si*	*Mo*	*V*	*Nb*	*N*	*Ni*	*Al*	*(Mn+Ni)*
		0.08–0.13	*1.20 max*	*8.0–10.5*	*0.15–0.50*	*0.85–1.2*	*0.15–0.30*	*0.02–0.10*	*0.03–0.07*	*0.8 max*	*0.04 max*	*1.4 max*
250°C Preheat												
PH 1	No alloying	0.090	0.48	8.40	0.28	0.97	0.22	0.081	0.052	0.35	0.005	0.83
PH 2	(0.5)Cr	0.089	0.47	8.88	0.28	0.97	0.22	0.077	0.051	0.36	0.004	0.83
PH 3	(1)Cr	0.087	0.47	9.47	0.28	0.97	0.22	0.078	0.054	0.36	0.005	0.83
PH 4	(2)Cr, (2)Mn	0.085	1.08	10.01	0.28	0.96	0.22	0.079	0.053	0.34	0.005	1.42
PH 5	(2)Cr, (1)Mn, (1)Mo	0.085	0.75	10.33	0.28	1.32	0.22	0.078	0.055	0.34	0.006	1.09
PH 6	(1)Cr, (1)Mn, (0.5)Ni	0.087	0.81	9.39	0.27	0.96	0.22	0.079	0.053	0.52	0.003	1.33
No Preheat												
AW 1	No alloying	0.090	0.48	8.61	0.31	0.94	0.22	0.088	0.056	0.35	0.003	0.83
AW 2	(1)Cr	0.100	0.48	9.12	0.30	0.93	0.21	0.082	0.055	0.35	0.004	0.83
AW 3	(2)Cr	0.100	0.49	10.3	0.29	0.94	0.22	0.086	0.059	0.36	0.010	0.85
AW 4	(2)Cr, (0.5)Mo	0.094	0.47	10.2	0.25	1.05	0.22	0.082	0.065	0.36	0.003	0.83
AW 5	(2)Cr, (1)Mo	0.090	0.48	10.2	0.30	1.37	0.22	0.088	0.057	0.35	0.006	0.83
AW 6	(2)Cr, (0.5)Ni	0.089	0.47	10.3	0.24	0.94	0.23	0.082	0.070	0.54	0.003	1.01
AW 7	(2)Cr, (1)Ni	0.100	0.48	10.3	0.30	0.91	0.22	0.083	0.057	1.13	0.005	1.61
AW 8	(2)Cr, (2)Ni	0.080	0.48	10.2	0.28	0.90	0.21	0.085	0.057	1.39	0.006	1.87
AW 9	(2)Cr, (1)Si	0.088	0.46	9.95	0.47	0.92	0.23	0.086	0.069	0.34	0.005	0.80
AW 10	(2)Cr, (2)Si	0.080	0.47	10.1	0.69	0.89	0.22	0.089	0.056	0.34	0.006	0.81
AW 11	(2)Cr, (2)Mn	0.100	1.16	9.74	0.29	0.92	0.22	0.083	0.059	0.35	0.004	1.51
AW 12	(2)Mn, (0.5)Mo	0.091	1.11	8.39	0.24	1.13	0.23	0.080	0.062	0.36	0.002	1.47
AW 13	(2)Mn, (1)Si	0.088	1.12	8.38	0.42	0.95	0.23	0.084	0.063	0.36	0.002	1.48
AW 14	(0.5)Mo, (1)Si	0.085	0.47	8.42	0.48	1.05	0.23	0.083	0.061	0.35	0.003	0.82
AW 15	(2)Cr, (0.5)Mo, (1)Si	0.085	0.46	9.18	0.45	1.02	0.23	0.089	0.060	0.35	0.004	0.81
AW 16	(2)Cr, (1)Mo, (1)Si	0.082	0.46	9.81	0.45	1.15	0.23	0.086	0.060	0.35	0.003	0.81
AW 17	(2)Cr, (1)Mo, (2)Si	0.100	0.46	9.92	0.58	1.20	0.22	0.085	0.056	0.34	0.005	0.80
AW 18	(2)Cr,(0.5)Mo, (1)Mn	0.102	0.79	10.3	0.23	1.02	0.22	0.078	0.070	0.36	0.003	1.15
AW 19	(2)Cr, (1)Mo, (1)Mn	0.120	0.91	9.71	0.29	1.34	0.22	0.086	0.059	0.34	0.008	1.25
AW 20	(2)Cr, (0.5)Mo, (0.5)Ni	0.088	0.47	9.55	0.25	1.03	0.23	0.083	0.059	0.54	0.003	1.01
AW 21	(2)Cr, (1)Mn, (1)Si	0.081	0.78	9.94	0.43	0.93	0.23	0.085	0.061	0.35	0.004	1.13
AW 22	(0.5)Mo, (2)Mn, (1)Si	0.081	1.13	8.27	0.50	1.04	0.23	0.088	0.065	0.35	0.003	1.48

of re-austenitisation and the formation of fresh martensite. Generally, increased amounts of δ-ferrite were observed in welds with higher Ae_1 due to higher Cr content in the weld beads. The amount of δ-ferrite was observed to also increase with Ae_3 temperatures. Application of 250 °C preheating decreased the minimum Ae_4 temperature required to suppress δ-ferrite from 1260 to 1230 °C. Generally, the δ-ferrite was observed to decrease with increasing Ae_4 temperature.

The relationship between the $(Ae_4 - Ae_3)$ temperature range and the amount of δ-ferrite in the final microstructure of the welds was examined, as shown in Fig. 5. Arivazhagan and Kamaraj [21] stated that the probability of δ-ferrite retention in the weld increases with a lower value of $(Ae_4 - Ae_3)$. Results of previous work on shielded metal arc welding (SMAW) beads [9] are incorporated in Fig. 5 and show good agreement with the present GMAW results on beads deposited without preheating. An $(Ae_4 - Ae_3)$ temperature range above 415 °C for welds that are not preheated seems to be necessary to suppress δ-ferrite in the as-welded microstructure. The required $(Ae_4 - Ae_3)$ range decreased to 385 °C when 250 °C preheating was applied. These results indicate that both the chemical composition, which

Table 3 Empirical formulation values based on gas–metal arc weld composition and observed percentage of δ-ferrite in weld microstructure (95% confidence interval). Values above the recommended limits (indicative of the risk of δ-ferrite) are highlighted in red

Weld ID	Schneider			Kaltenhauser	Newhouse	Measured δ-ferrite content	Weld microstructure prediction
	Cr_{eq} (≤ 13.5)	Ni_{eq}	FF (≤ 8)	KFF (≤ 8)	CNB (≤ 10)		
250 °C Pre-heat							
PH 1	11.7	4.6	7.0	7.0	9.3	0.0	✓
PH 2	12.1	4.6	7.6	7.5	9.8	0.0	✓
PH 3	12.7	4.6	**8.1**	**8.1**	**10.4**	0.0	×(c)
PH 4	13.2	4.8	**8.5**	7.5	9.8	0.3 ± 0.1	✓
PH 5	**14.1**	4.7	**9.4**	**9.8**	**12.2**	3.5 ± 0.9	✓
PH 6	12.6	4.9	7.7	6.9	8.9	0.0	✓
No Pre-heat							
AW 1	11.9	4.7	7.2	7.1	9.4	0.0	✓
AW 2	12.3	5.0	7.3	7.1	9.3	0.5 ± 0.1	×(nc)
AW 3	**13.6**	5.1	**8.4**	**8.1**	**10.4**	1.4 ± 0.4	✓
AW 4	13.5	5.1	**8.5**	**8.2**	**10.6**	1.9 ± 0.5	✓
AW 5	**14.1**	4.7	**9.3**	**10.3**	**12.6**	4.3 ± 0.6	✓
AW6	13.4	5.3	**8.2**	7.3	9.5	1.0 ± 0.2	✓
AW 7	13.5	5.8	7.7	6.6	7.4	0.0	✓
AW 8	13.3	5.5	7.8	6.6	6.7	0.0	✓
AW 9	**13.6**	5.0	**8.6**	**8.9**	**11.5**	3.8 ± 0.6	✓
AW 10	**14.1**	4.4	**9.7**	**11.1**	**13.5**	2.2 ± 0.7	✓
AW 11	12.9	5.4	7.5	6.0	8.4	0.4 ± 0.15	×(nc)
AW 12	11.9	5.2	6.6	5.6	8.1	0.0	✓
AW 13	11.9	5.2	6.8	6.0	8.5	0.0	✓
AW 14	12.3	4.7	7.6	**8.4**	**10.9**	0.13 ± 0.06	✓
AW 15	12.9	4.6	**8.3**	**8.9**	**11.4**	1.1 ± 0.3	✓
AW 16	**13.7**	4.6	**9.2**	**10.2**	**12.6**	6.0 ± 1.1	✓
AW 17	**14.1**	5.0	**9.1**	**10.7**	**13.1**	6.2 ± 1.2	✓
AW 18	13.5	5.7	7.8	6.7	9.2	1.8 ± 0.4	×(nc)
AW 19	**13.6**	5.9	7.7	7.5	9.9	2.4 ± 0.5	✓
AW 20	12.9	4.9	8.0	7.6	9.7	0.3 ± 0.14	×(nc)
AW 21	13.5	4.7	**8.8**	**8.6**	**11.2**	2.6 ± 0.6	✓
AW 22	12.1	5.0	7.1	7.0	9.5	0.0	✓

(✓) Presence or absence of δ-ferrite was correctly predicted. (**x**(c)) Presence or absence of δ-ferrite was incorrectly predicted (conservative). (**x**(nc)) Presence or absence of δ-ferrite was incorrectly predicted (not conservative).

determines the ($Ae_4 - Ae_3$) temperature range, and the cooling rate through this temperature range are important in suppressing δ-ferrite in the final as-welded microstructure [14].

3.5 Prediction of as-welded microstructure from empirical formulae

Schaeffler, Schneider, Kaltenhauser, and Newhouse formulae (Eqs. 6 to 11) were applied to calculate the empirical values based on the GMAW chemical composition.

Schaeffler modified formulae:

$$Cr_{eq} = Cr + 1.5Si + Mo + 0.5Nb + 0.75W \quad (6)$$

$$Ni_{eq} = Ni + 0.5Mn + 30C + 30N + 0.3Cu + Co \quad (7)$$

Schneider formulae:

$$Cr_{eq} = Cr + 2Si + 1.5Mo + 5\,V + 1.75Nb + 0.75W \quad (8)$$

$$Ni_{eq} = Ni + 0.5Mn + 30C + 25N + 0.3Cu \quad (9)$$

Kaltenhauser formula:

$$(KFF) = Cr + 6Si + 4Mo + 4Nb + 2Al + 8Ti - 2Mn - 2Ni - 40(C + N) \quad (10)$$

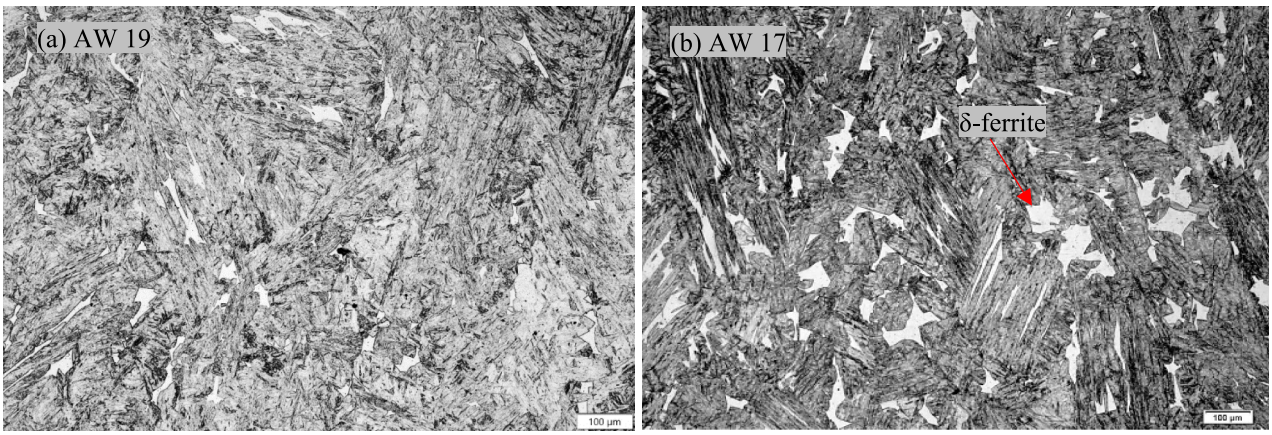

Fig. 4 Optical microstructure images of **a** AW 19 weld bead containing 2.4% δ-ferrite and **b** AW 17 containing 6.2% δ-ferrite, in a martensitic matrix in as-welded condition (100 × magnification)

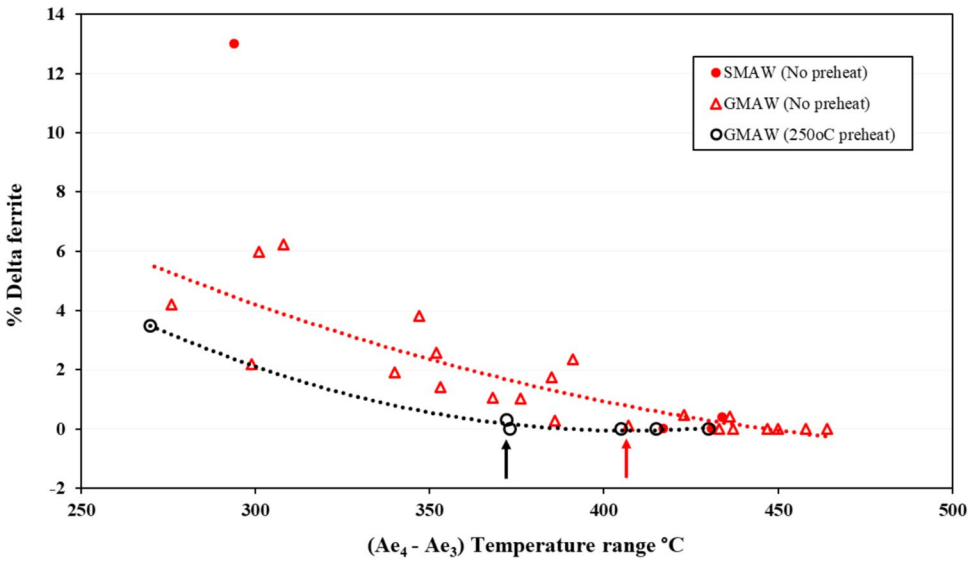

Fig. 5 Relationship between ($Ae_4 - Ae_3$) temperature range and amount of delta ferrite in the final microstructure of weld. The red and black arrows indicate the estimated ($Ae_4 - Ae_3$) values necessary to suppress delta ferrite without and with preheating, respectively [14]

Newhouse formulae:

$$CBN = Cr + 6Si + 4Mo + 1.5W + 5Nb + 9Ti + 11V + 12A1 - 40C - 30N - 2Mn - 4Ni - 1Cu \quad (11)$$

The correct or incorrect prediction of GMA welds microstructure by the various empirical formulae is indicated in Table 3, as well as the percentage volume fractions of δ-ferrite. The highlighted values are above the recommended limits that predict the presence of δ-ferrite in the P91 as-welded microstructure. Five welds, namely, PH 3, AW 2, AW 11, AW 18, and AW 21, were incorrectly predicted by all empirical formulae. PH 3, which received 250 °C preheating, consisted of a fully martensitic structure, contrary to prediction. The remaining four welds were predicted to be fully martensitic, yet δ-ferrite was observed in their microstructures. Eighteen of the 28 welds (64%) were correctly predicted by all empirical formulae.

Cr_{eq} is plotted against the amount of δ-ferrite in Fig. 6. For the Schaeffler Cr_{eq}, a steep increase was observed from 11.5, which is below the 12.5 limit recommended by Faulkner [22]. Based on these results, the recommended Schaeffler Cr_{eq} value to limit the presence of δ-ferrite in P91 GMA welds should be lowered to 11.5. A steep increase in δ-ferrite content was observed above the recommended Schneider Cr_{eq} of 13.5, indicated by the broken red line in Fig. 6.

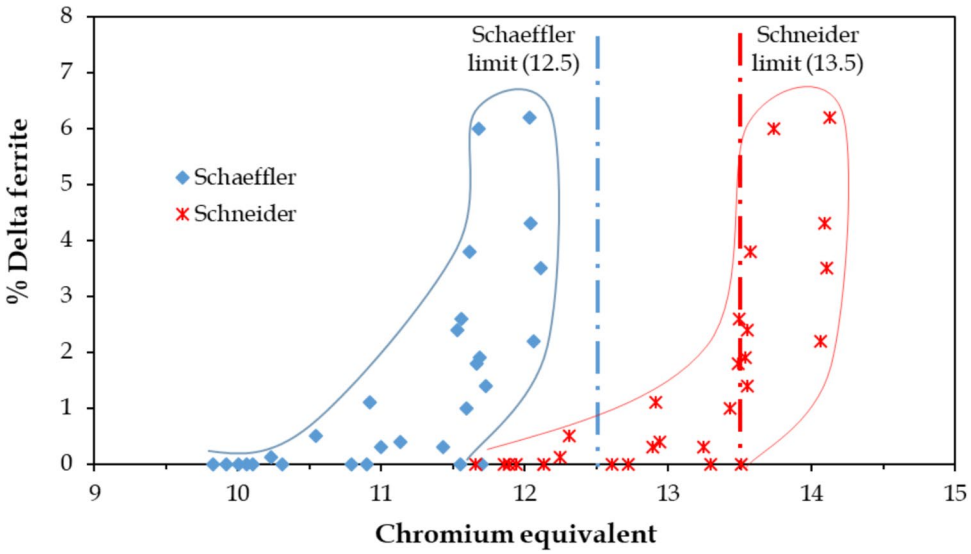

Fig. 6 Effect of Cr_{eq} on δ-ferrite in deposited gas–metal arc as-welded metal

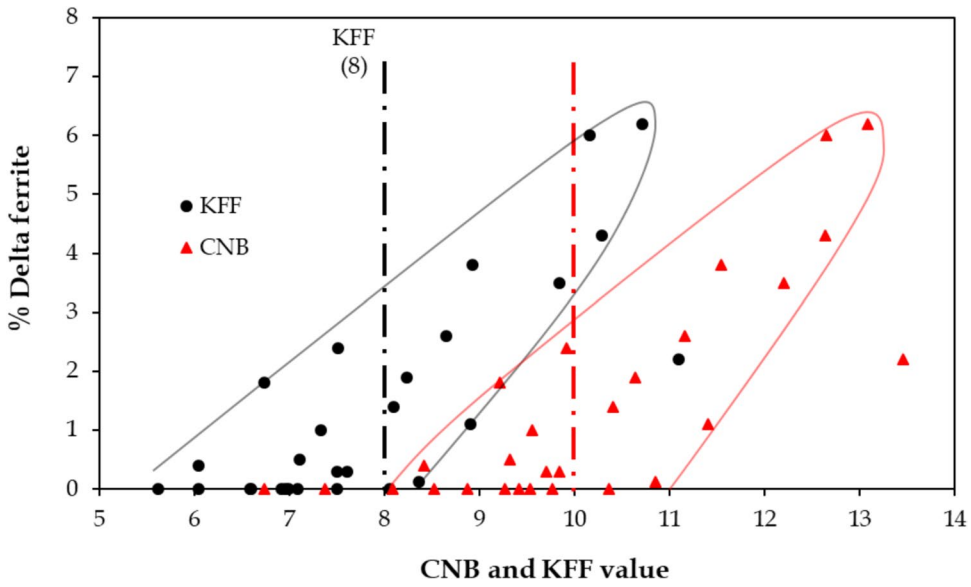

Fig. 7 Effect of Kaltenhauser ferrite factor (KFF) and chromium-nickel balance (CNB) on δ-ferrite content in deposited gas–metal arc as-welded metal

Figure 7 shows a lot of scatter in the data, but a trend of increasing amounts of δ-ferrite with Kaltenhauser ferrite factor (KFF) and CNB is observed. Several welds with δ-ferrite were observed with KFF below the limit of 8, recommended by Sireesha et al. [23]. The results in Fig. 7 agree with Barnes et al. [24], who recommended that a KFF limit of 6 is necessary to achieve fully martensitic P91 welds. Delta-ferrite was observed in seven welds with CNB < 10, which is the limit recommended by Swindeman et al. [25].

These results show that these empirical formulae cannot exclusively be relied upon to accurately predict weld microstructures with the current recommended limits, especially where small amounts of δ-ferrite are probable.

3.6 Effect of thermal cycle on delta ferrite in a multi-pass weld

The objective of the Gleeble thermal treatment simulation experiment was to evaluate the effect of a subsequent bead thermal cycle on the morphology and volume fraction of δ-ferrite in a previously deposited weld bead. The microstructure of the five welds in the as-welded condition consisted of a martensitic matrix with δ-ferrite ranging from 1.8 to 6%. A trend of lower δ-ferrite was observed in Gleeble specimens treated at peak temperatures of 900 and 1100 °C, as shown in Fig. 8. The Gleeble thermal peak temperatures of 900 °C and 1100 °C were within the (Ae_3–Ae_4)

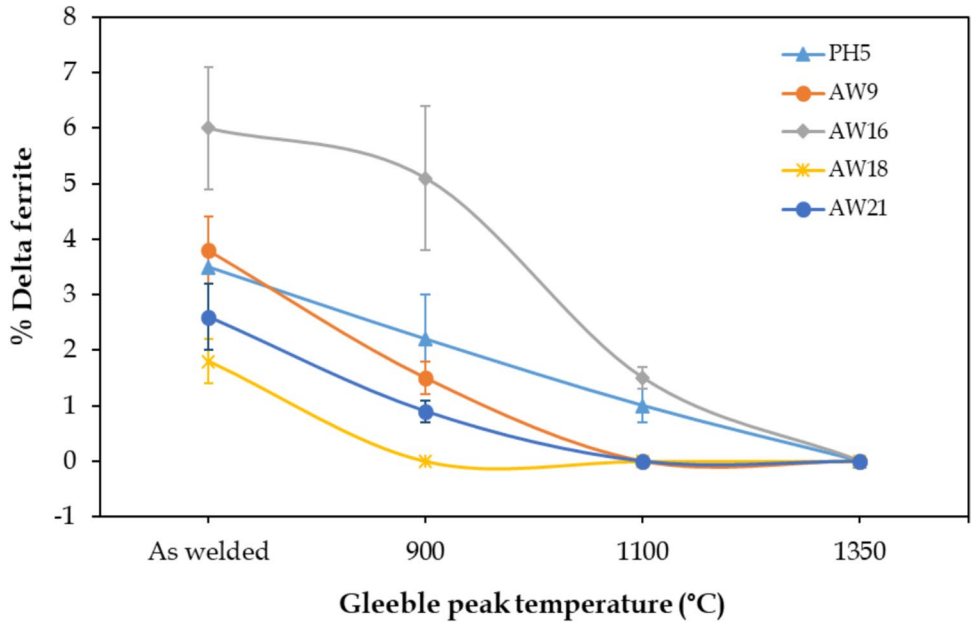

Fig. 8 Change in δ-ferrite content with Gleeble thermal treatment

temperature range where only austenite phase is stable, and no δ-ferrite was expected. These results suggest that the amount of δ-ferrite can be reduced by applying a subsequent bead or temper bead.

4 Implications of results for practical welding of P91 steel

4.1 Weld composition

(i) In this study, 81% of welds that complied with the composition specification contained δ-ferrite. The AWS A5.28/A5.28 M:2022 (ER90S-B91) specification limits may need to be revised to ensure a fully martensitic microstructure. Table 4 shows the proposed changes to the current specification. Mo and Si are ferrite-formers so these limits are proposed to be lowered. Changes in Cr limits are not recommended, even though it is a strong ferrite-former, because it is the main alloying element in P91 steels, having an important role in elevated-temperature strength properties and in improving resistance to oxidation and corrosion. Ni is a strong austenite-former, so it is proposed that a lower limit should be specified to ensure that it is present in sufficient quantities in the weld.

(ii) Qualification of the filler material is recommended. Before using a batch of welding consumables, testing of the weld metal composition to ensure that Schaeffler $Cr_{eq} < 11.5$ and analysis of the as-welded microstructure to confirm the absence of δ-ferrite are recommended.

Table 4 Proposed changes to chemical composition range limits of AWS A5.28/A5.28 M:2022 (ER90S-B91) and ISO 21952:2012 (CrMo91) specifications

Element	*P91 weld metal (%)*		
	AWS A5.28:2022 (ER90S-B91)	*ISO 21952:2012 (CrMo91)*	*Recommended changes**
	Min – max	*Min – max*	*Min – max*
C	0.07 – 0.13	0.07 – 0.15	
Mn	– 1.20	0.40 – 1.50	– 1.20
Cr	8.00 – 10.50	8.00 – 10.50	
Si	0.15 – 0.50	– 0.60	0.15 – 0.35
Mo	0.85 – 1.20	0.80 – 1.20	0.70 – 1.00
V	0.15 – 0.30	0.15 – 0.30	
Nb	0.02 – 0.10	0.03 – 0.10	
N	0.03 – 0.07	0.02 – 0.07	
Ni	– 0.80	0.40 – 1.00	0.40 – 0.80
Al	– 0.04		

** Schaeffler $Cr_{eq} \leq 11.5$ is recommended*

4.2 Cooling rate

There are two main welding implications derived from this study in relation to the cooling rate.

(i) Firstly, in a single-pass welding process, lower cooling rates resulted in a decreased amount of δ-ferrite in the as-welded microstructure. This is

because the diffusion-controlled transformation of δ-ferrite to austenite is afforded time above the Ae_3 temperature to proceed to completion. It is therefore recommended to use high heat input (minimum 1.4 kJ/mm when pre-heating is applied) in single-pass welds.

(ii) Secondly, in multi-pass welds simulated by Gleeble experiment, the subsequent bead thermal cycle decreased the δ-ferrite content in the microstructure of previously deposited beads. This was because, in multi-pass weld, the amount of δ-ferrite that forms from austenite during heating in the bead overlaid by subsequent passes depends on the time spent above the Ae_4 temperature. Low heat input in subsequent beads will limit the δ-ferrite in previously deposited beads.

Applying temper beads can be beneficial in decreasing δ-ferrite in previously laid beads.

5 Conclusions

(i) Compliance of a weld metal chemical composition to the AWS A5.28/A5.28 M:2022 (ER90S-B91) and ISO 21952:2012 (CrMo91) specification ranges does not ensure a fully martensitic microstructure. Of the GMA welds that complied with the composition specifications, 81% contained δ-ferrite in their microstructure. To quote extreme examples, AW 9 and AW 16 contained 3.8% and 6% δ-ferrite, respectively, yet their compositions were within the specification limits.

(ii) Empirical formulae cannot exclusively be relied upon to accurately predict weld microstructures with the current recommended limits, especially where small amounts of δ-ferrite are probable. The prediction accuracy of the empirical formulae improved in welds containing > 1% δ-ferrite.

(iii) An $(Ae_4 - Ae_3)$ temperature range > 415 °C for P91 welds that were not preheated was necessary to suppress δ-ferrite in the as-welded microstructure. This value decreased to 385 °C when 250 °C preheating was applied. These results indicate that both the chemical composition which determines the $(Ae_4 - Ae_3)$ temperature range and the cooling rate through this temperature range are important in suppressing δ-ferrite in the final as-welded microstructure.

(iv) Significant reduction in δ-ferrite was observed in Gleeble specimens treated at peak temperatures of 900 °C and 1100 °C; no δ-ferrite was observed for 1350 °C peak temperature. Gleeble results indicated that the amount of δ-ferrite can be reduced by applying a subsequent bead or temper bead.

Acknowledgements We acknowledge the following companies and people for assistance: SecMet for providing the P91 base material, Corney van Rooyen and Maritha Theron at the South African Council for Scientific and Industrial Research (CSIR) for assistance with the laser metal deposition and providing some of the alloying elements, Steinmüller Africa for donating the welding consumable, and Prof. Kathy Sole for editorial assistance with the manuscript.

Author contribution Sibusiso Mahlalela and Pieter Pistorius contributed equally to conducting the experiments and writing the manuscript.

Funding Open access funding provided by University of Pretoria. Authors 1 and 2 received financial support from the Southern African Institute of Welding.

Data availability Not applicable.

Declarations

Competing interests The authors declare no competing interests.

Employment I am an employee of the University of Pretoria, South Africa.

References

1. Pandey C, Mohan Mahapatra M, Kumar P, Saini N (2018) Autogenous tungsten inert gas and gas tungsten arc with filler welding of dissimilar P91 and P92 steels. J Press Vessel Technol 140:2. https://doi.org/10.1115/1.4039127
2. Anderko K, Schäfer L, Materna-Morris E (1991) Effect of the δ-ferrite phase on the impact properties of martensitic chromium steels J Nucl Mater: Part 1 179(Part 1):492–495
3. Abe F, Araki H, Noda T, Okada M (1988) Microstructure and toughness of Cr-W and Cr-V ferritic steels. J Nucl Mater 155:656–661
4. Liu XY, Fujita T (1989) Effect of chromium content on creep rupture properties of a high chromium ferritic heat resisting steel. ISIJ Int 29(8):680–686
5. Laha K, Chandravathi K, Rao KBS, Mannan S (1995) Hot tensile properties of simulated heat-affected zone microstructures of 9Cr 1Mo weldment. Int J Press Vessels Pip 62(3):303–311
6. Kobayashi S, Sawada K, Hara T, Kushima H, Kimura K (2014) The formation and dissolution of residual δ ferrite in ASME Grade 91 steel plates. Mater Sci Eng: A 592:241–248. https://doi.org/10.1016/j.msea.2013.10.058
7. Yoshizawa M, Igarashi M (2007) Long-term creep deformation characteristics of advanced ferritic steels for USC power plants. Int J Press Vessels Pip 84(1):37–43

8. Abson DJ, Rothwell JS (2013) Review of type IV cracking of weldments in 9–12%Cr creep strength enhanced ferritic steels. Int Mater Rev 58(8):437–473
9. Mahlalela SS, Pistorius PGH (2022) Investigation of δ-ferrite content in weld metal of modified 9Cr–1Mo electrodes using thermodynamic modelling and quenching experiments. Weld World 66(6):1191–1198
10. Arivazhagan B, Kamaraj M (2013) Metal-cored arc welding process for joining of modified 9Cr-1Mo (P91) steel. J Manuf Process 15(4):542–548
11. Sam S et al (2014) Delta ferrite in the weld metal of reduced activation ferritic martensitic steel. J Nucl Mater 455(1–3):343–348
12. Abd El-Rahman Abd El-Salam M, El-Mahallawi I, El-Koussy M (2013) Influence of heat input and post-weld heat treatment on boiler steel P91 (9Cr–1Mo–V–Nb) weld joints Part 1–Microstructure. Int Heat Treat Surf Eng 7(1):23–31
13. Arivazhagan B, Srinivasan G, Albert SK, Bhaduri AK (2011) A study on influence of heat input variation on microstructure of reduced activation ferritic martensitic steel weld metal produced by GTAW process. Fusion Eng Des 86(2):192–197
14. Mahlalela S, Pistorius P (2023) Influence of alloying elements and cooling rate on the presence of delta ferrite in modified 9Cr–1Mo as-welded microstructure produced by gas–metal arc welding. Weld World 1–12
15. Phelan D, Reid M, Dippenaar R (2006) Kinetics of the peritectic phase transformation: in-situ measurements and phase field modeling. Metall and Mater Trans A 37:985–994
16. International Organization for Standardization (ISO21952:CrMo91) (2007) Welding consumables—wire electrodes, wires, rods and deposits for gas shielded arc welding of high strength steels—classification.
17. American Welding Society A5.28/A5.28M:2022 (ER90S-B91), Specification for low-alloy steel electrodes and rods for gas shielded arc welding. An American National Standard, Miami, FL.
18. Thermo-CalcSoftware. (2023, January 23, 2024). TCS steel and Fe-alloys database (TCFE13). Available: https://thermocalc.com/products/databases/steel-and-fe-alloys/
19. Dupont JN, Marder AR (1995) Thermal efficiency of arc welding processes. Welding Journal-Including Welding Research Supplement 74(12):406s
20. Villaret F, Boulnat X, Aubry P, Zollinger J, Fabrègue D, de Carlan Y (2021) Modelling of delta ferrite to austenite phase transformation kinetics in martensitic steels: application to rapid cooling in additive manufacturing. Materialia 18:101157
21. Arivazhagan B, Kamaraj M, (2023) A study on influence of D-ferrite phase on toughness of P91 steel welds. White Paper, Steel-Grips. Com, pp 19–24
22. Faulkner R, Williams J, Sanchez EG, Marshall A (2003) Influence of Co, Cu and W on microstructure of 9% Cr steel weld metals. Mater Sci Technol 19(3):347–354
23. Sireesha M, Sundaresan S, Albert SK (2001) Microstructure and mechanical properties of weld fusion zones in modified 9Cr-1Mo steel. J Mater Eng Perform 10(3):320–330
24. Barnes A, (1995) The effect of composition and heat treatment on the microstructure and mechanical properties of modified 9Cr 1Mo weld metal. TWI Members Report
25. Swindeman RW, Santella ML, Maziasz PJ, Roberts BW, Coleman K (2004) Issues in replacing Cr-Mo steels and stainless steels with 9Cr-1Mo-V steel. Int J Press Vessels Pip 81(6):507–512